

Theoretical Model To Calculate Aerodynamic Interference Effects Between Rotor And Wing Of Tiltrotors

A. Lesching, S. Wagner

Institut für Luftfahrttechnik und Leichtbau
Universität der Bundeswehr München
Werner-Heisenberg-Weg 39
D - 8014 Neubiberg / West-Germany

Abstract

The aerodynamic interactions between the rotor and the wing of a tilt-rotor configuration are discussed in both hover and forward flight. The procedure contains a vortex lattice representation of the wing and the rotor and is fully coupled to get the loads on both systems. Results are presented for hover and forward flight condition for the isolated rotor and the rotor plus wing configuration. It is shown, that the interaction has a significant effect on the integrated wing and rotor loading. On the other hand the effect on the power required is small. The flow field in the region of possible tail location is represented.

Introduction

The development of the tilt-rotor aircraft results in a vehicle, which combines the low speed hover capabilities of a helicopter with the high speed flight capabilities of a fixed wing aircraft. A complete knowledge of the aerodynamic interaction between the major components is essential to understand its performance. In particular, the fundamental flow field effects between the rotor and the wing are of great interest for future improvements in the configuration concepts.

The analytical modeling of the full helicopter flow field with rotor and fuselage was impossible, due to limitations in the computing facilities and complexity of the problems. Some research work has already been performed on the rotor / wing interference, e.g. Ref. (1,2,3,4). Typically, pure wake models consist of prescribed wakes (Ref. 5,6), which are

based on special helicopter rotor conditions with linear twist distributions and low thrust values. Recently an analytical model (Ref. 7) of the rotor/wing problem was presented, which includes the rotor as a disc and connects a time averaged vortex sheet model of the rotor wake to get the loads of the system using the blade element method.

The present method has the capability to determine the fully coupled aerodynamic response of a rotor with several blades and a wing to show the interference effects on each rotor blade. It is useful to study the flow field details at every point of the surrounding domain. The method is based on the VLM-Method (Vortex Lattice Method Ref. 8), which is able to calculate the airloads of each rotor blade and the wing and to represent steady and quasisteady flow conditions. The approach includes the general flow field modeling capability of a panel method and allows to determine regions of separated flow. It can also model the aerodynamic interaction of fixed components of the system. Including nonlinear inflow, the consequence is the determination not only of rotor downwash on the horizontal and vertical stabilizers, but also the effect of wing induced up- and downwash on the rotor forces and rotor moments.

The paper contains a preliminary study of the interference between rotor and wing of a tilt-rotorsystem. Data from actual projects are used to show the results for the isolated rotor, the wing/rotor combination in hover and in forward flight for a representative advance ratio. The loading of each rotor blade, the

integrated rotor and wing forces and the representation of the flow phenomena are summarized in the calculation process. The study of the flow field characteristics shows the substantial interference between the wing and the rotor in hover. The interaction in forward flight is low in spite of the forward velocity on the rotor, but the wing loading experiences a significant modification. The wake vorticity from wing and rotor are swept aft quickly. In the present version of the program no attempt has been made to get the aerodynamic interference effect of the fuselage system on the rotor loading.

Basic Method

The present rotor version offers a full description of the highly interactive flow field between the rotor and upstream existing components of the system. The rotor wake of each blade and the wing are represented by a time dependent, quasi steady Vortex Lattice Method, which includes the Kutta condition at the trailing edge and fulfills the irrotational, isentropic full potential equation. Existing instability effects are represented in the development of the free wake vortex modeling. No external specification of the strength of the vortex sheets and of the location is required. The wake is free of force.

The wake length increases during the computational process. The circulation distribution and the inflow are calculated in each cycle. When the aerodynamic loading reaches a quasi steady solution for the rotor and the wing, the values are fed into another program, where the spanwise loading is summarized to obtain the integrated forces and moments by the blade element theory. The performance iteration is started again until no difference exists between the actual and the desired trim parameters. This is illustrated schematically in figure 1. The rotor wake developing from the starting process is represented by vortex rings, which are included in the calculation method.

Whenever in the wake modeling phase the wake "bulb" is created, it will be substituted by vortex rings and combined with the older ones. The conservation of circulation is guaranteed in the present version of the program.

The rotor model

For the preliminary study of the rotor behaviour a representative tilt-rotor was used. It is the 3-bladed XV-15 rotor with a solidity of 0.1 and a nonlinear twist distribution (Ref. 9). The blade chord is nearly linear and the assumed tip Mach number is 0.66 for the hover case. The coordinate system is located to the center of the rotor. The discretisation is outlined in figure 2. The blade is divided into a mesh of cells in spanwise and chordwise direction, the circulation of the vortex filament is constant inside the cell, but may change from one cell to its neighbouring one.

In the present paper only cases of one cell in chordwise direction is dealt with. During the development of the wake with the VLM-method the free trailing vortices move away from the rotor disc and reach another position after each time step. From figure 3 one can see the created wake bulb, which exists after some iteration loops. The program substitutes these wake elements in the bulb by vortex rings, an inner and outer one for each blade, which includes all the circulation.

Depending on the test case, it is always necessary to have available 1 to 1.5 revolutions of free wake elements resulting from the rotor blade, when starting the substitution routine, otherwise the rotor blade circulation does not reach a quasi steady solution. The calculation process continues until a new wake bulb is created. The substitution routine models again vortex rings and combines the new with the older one to reach the same amount of rings as previously. The effect of using such a modeling technique is a reduced computation time, which will be

discussed later in this paper. As shown in figure 4, the rotor and its wake is represented in the computational module by 24 cutting planes, which are limited in radial direction to the rotor radius R and are unlimited in z direction. It is checked, whether the wake elements of each rotor blade passes the modeled cutting plane in flow direction on the lefthand or righthand side of the maximum of circulation. All intersection points with the actual vortex strength are summarized and a final location of the inner and outer vortex rings is computed for each plane. Finally the outlined procedure represents the position and the strength of all vortex rings.

The rotor/wing model in hover

For the hover case a tilt-rotor configuration is used similiar to the one of Ref. (7). The wing has an aspect ratio of 5 with constant chord and with no dihedral. Its angle is about 5°. The rotor with a radius of 40% of the wing span was positioned with its axis at the wing tip leading edge and rotated in a plane parallel to, and roughly 85%, of the wing chord above the wing pitch axis. The 3-bladed rotor has linear twist distribution of 40° and a solidity of 0.1. As shown in figure 5, the blade chord is to be constant to mid-radius, then tapered to 25% of the root chord at the tip.

The panel model of the rotor is the same as for the single rotor calculation. The wing is modeled with the vortex lattice method, which is schematically shown in figure 6. The circulation of each elementary wing is represented by a horseshoe vortex. The sharing of the bound vorticity of each elementary wing is located at the 25%-line. The free trailing vortices leave each cell as semi-infinite vortices. The horseshoe vortex fulfills the Helmholtz vortex theory. At the control points, the tangential flow condition is fulfilled. Its location is the midpoint of the last elementary wing at the trailing edge. The vortex lattice is produced by the horseshoe vortices in

chordwise direction. The rows are identical with the bound vortices and both spars of each elementary wing correspond to the free trailing vortices. The circulation distribution in chordwise direction is adapted to the thickness of the wing profile. A detailed description of this method is outlined in Ref (10).

The rotor/wing model in forward flight

The forward flight case was configured for the XV-15 with an advance ratio of 1.67. The coordinate system is fixed to the rotor center and the wing was located in upstream direction as shown in figure 7. The wing chord length is about 1.59 m, the incidence angle is 3°, and the section has a forward sweep of 6° 3' at the quarter chord line. The rotor has one panel in chordwise direction. The wing geometry is represented by a thin surface composed of a number of conveniently chosen trapezoidal panels (figure 8).

The difference to the model in hover case is the usage of 6 vortex boxes, which are produced by the vortex filaments. The bound circulation of each panel is considered uniform and it is noted, that the pressure coefficient across the lifting surface must smoothly approach zero at the trailing edge and remain so across the force free wake surface. With the present method it is possible to model every wing geometry in positioning the surface panels at the chord line. At the mid of each vortex box (control point) the normalwash from each blade surface is equalized to the normal component of the free-stream. Thus a set of equations in the form

$$\sum A_{ij} \cdot \mu_i = RS_i \quad (1)$$

is established. The aerodynamic influence coefficient A_{ij} combines the influence of all vortex boxes. μ_i is the vortex strength at the control point i. The influence of the wake is included in the right side (RS) of equation 1 and is calculated analytically by the application of the

Bio-Savart law in Cartesian vector form. Plus the freestream velocity at each point i the circulation distribution can be found with an appropriate technique to solve linear equations. The explanation of the solution procedure is outlined in Ref. (8).

The calculation procedure

The calculation process begins with an initial setting of the collective and cyclic pitch. For the hover case of the rotor/wing combination one rotor calculation cycle is first carried out with these values, then the calculation of the rotor forces and moments are modeled with the circulation distribution of each blade. If required, the blade flapping can be included. The calculated thrust is compared with the target value and the collective pitch adjusted as appropriate. With the new collective pitch setting the loop starts again until the trim parameters are stabilized within a tolerance limit. When this condition is reached, the wake calculation process continues with the last trim values.

The substitution in hover of the wake bulb by vortex rings proceeds until the rings have a distance in z direction of about 1 rotor radius from the location of the wing. From now the wake development of the wing starts in order to get its interference effect for the rotor loading distribution. Experience with a variety of rotor types and conditions has shown, that, in hover case, 2 revolutions of the rotor are adequate to stabilize the rotor loads. Whenever the rotor wake passes the wing, a special module changes the path of the filaments and adapts them to the contour of the wing. By this procedure, the rotor wake has no chance to cut the doublet elements of the wing. In the forward flight case, the wing wake develops at the beginning of the calculation process. The rotor wake is modified when reaching the wing area. In both cases the nonuniform rotor inflow, includ-

ing the effect of the wing, can be modelled with no difficulty.

Discussion of the results

In table 1 the configuration build-up and the flight conditions are given for the analyzed flight cases.

Hover case for the XV-15

The initial pitch settings are similar to those mentioned in Ref. (9). The aim for the hover case of the XV-15 is to analyze the results for the induced velocity distribution with the present wake modul. Without the vortex ring technique the computation time is too large for usage in the trim iteration procedure. As shown in figures 9a,b, the wake shape and the circulation distribution have reached a steady solution. When using the outlined vortex ring modeling, the computation time was reduced to 15% of the original time. Figure 10 shows the wake representative for only one rotor blade including the swept aft vortex rings. The shape is similar to the long original method. Figure 11 shows the angle of attack distribution over the rotor disc similar to the one typical for the hover case. The flow field under the rotor (figure 12) represents the location of the tip vortex and should have no influence on the aerodynamic loading of the rotor.

When comparing the induced velocity distribution at a level, where the wing is actually located, the results show good agreement with the experimental data (figure 13). The difference between the calculated and the measured data within the of 60 to 70 percent of the rotor radius depends on the structure of the wake shape, which may be influenced by the compressibility effects, which are not included in the present version of the program. The calculated figure of merit is excellently confirmed by the desired thrust coefficient (see diagram 14).

Hover flight case for rotor/wing

Studying the hover case for the combination rotor+wing, the wake shape shows differences in comparison with the isolated rotor (figure 15a,15b). The uniform shape is modified by the presence of the wing. Analyzing the circulation distribution of the rotor blade, the movement over the wing is combined with a higher circulation value than outside the wing area (see fig. 16). Examining this effect at the aerodynamic parameters, the influence of the wing can be outlined in the contours of the isolines. The blade angle of attack is higher on the wing side (see the dashed line in figs 17a,b) than on the opposite side, due to the lower induced velocity distribution. In figure 18a,b the symmetry in the rotor plane for the isolated rotor has changed to a nonsymmetric distribution.

The wing interference is better illustrated in figures 19a,b, which show the large perturbation in the azimuthal angle of attack distribution and the radial distribution as the blade sweeps over the wing. In both cases, the distribution for the isolated rotor is plotted for comparison. The unsteadiness in lift is increased, and it might be expected to cause increased vibrational loads. The asymmetric flow vector diagram 20 shows the influence of the tip vortex on the flow structure. On the righthand side, where the wing is located, the vortex is weaker than on the opposite side. The flow field experiences a large modification near the wing and influences the flow stream up.

In figure 21 the streamlines are shown for only a few time steps of the computational procedure. From their starting position they flow around the wing and leave the wing area without cutting it. When adding the wing, the overall power has a slightly effective influence. It is about 1.5% higher than without the wing.

Forward flight case rotor/wing

Placing the rotor at the tip of the wing as presented in case of the present study of the XV-15, the rotor/wing combination has very little effect on the overall rotor performance or on the blade section behaviour. The total rotor power coefficient c_p shows a small change in forward flight compared to the isolated rotor (figure 22). The initial parameters are outlined in table 1. The wake, produced by the rotor, leaves the rotor region quickly and is influenced by the present wing location. As shown in figure 23a, the vortex filaments, which pass the wing, are modified. The shape of the lefthand rotor wake is nonuniform and disturbed by the wing vortices. The circulation distribution at the rotor is represented in figure 23b. It is shown, that, after a few time steps, a steady solution is reached. In figure 24a and 24b the induced velocity distribution and the effective angle of attack are calculated in the rotor plane. The downward rotating blade experiences a local angle of attack increase, which increases the section lift resulting in an augmented thrust and torque on the blade. The upward rotating blade experiences a local angle of attack decrease which diminishes the section lift resulting in a decreased thrust and torque on the blade. The induced velocity distribution shows the opposite behaviour as the angle of attack.

In figure 25 the flow vectors behind the rotor/wing configuration are shown in the z-y plane. The location of the three strong tip vortices are represented and should influence the loading of the tail of tilt-rotor aircraft.

Figure 26 shows the typical section loading of the isolated wing and of the rotor/wing combination. In the upwash region the propeller swirl counteracts the effects of the wing downwash and the local angle of attack is increased. Simultaneously

the section lift augments and produces a higher wing lift than at the wing section, where no propeller is located. When considering conventional rotor / wing configurations for aircrafts, in the downward rotating region of the propeller, the local angle of attack at the wing will decrease, because the wing downwash and the propeller swirl act together. The positive effect on the upwash side will be reduced and the section lift is decreased. Taking this into account, it is easily apparent to locate the propeller at the wingtips as done with the XV-15. The propeller upwash region acts inboard the wing, the downwash side has no effect on the lift distribution. Similiar results are dicussed in Ref (11,12).

Conclusion

A coupled rotor/wing analysis using the VLM - method has been carried out for preliminary studies of the aerodynamic interference effects on rotor and wing in hover and forward flight case for representative tilt-rotor configurations. The changes in rotor blade loading are outlined whenever passing the wing. The asymmetric distribution of the aerodynamic parameters is shown. The effect of interaction is larger in hover than under normal forward flight condition. The influence of interference effect on the rotor performance appears small. Analyzing the flow field with the present method, regions of strongly varying flow have been identified. A detailed investigation of the flow phenomena for different configurations is possible for hover and forward flight cases. In future it will be necessary to reduce the computation time used for the trim iteration process. The compressibility effects, which are of minor influence in the present procedure, should be analyzed more accurately for the near field of the rotor wake.

Acknowledgement

The paper is partly based on research work founded by the Bundesminister

der Verteidigung BMVG (Ministry of Defence)

References

- [1] Brian Maskew, Use of Panel Methods in Helicopter Aerodynamics, Presented at the AHS Specialists Meeting on Aerodynamics and Aeroacoustics, Arlington, Texas, February 1987
- [2] Daniel J. Strash, James K. Nathman, Brian Maskew and Frank A. Dvorak, The Application of a Low Order Panel Method, Program VSAERO, to Powerplant and Airframe Flow Studies AIAA 842178 2nd Applied Aerodynamics Conference, Seattle, Washington August 1984
- [3] Michael A. McVeigh, Rotor / Airframe Interaction on Tilt-rotor Aircraft, Presented at the 44th Annual Forum and Technology Display of the American Helicopter Society, Washington D.C.
- [4] Fort F. Felker, Full-Scale Tilt Rotor Hover Performance, Presented at the 41th Annual Forum of the American Helicopter Society, Forth Worth, Texas, May 1985, Journal of the American Helicopter Society, April 1986
- [5] J.D. Kocurek and J.L. Tangler A Prescribed Wake Lifting Surface Hover Performance Analysis, American Helicopter Society 32nd Annual Forum, Washington, D.C., May 1976
- [6] A. Landgrebe, Overview of Helicopter Wake and Airload Technology, 12th European Rotorcraft Forum, Paper No.18 Garmisch Partenkirchen, FRG September 1986
- [7] David R. Clark, Analysis of the Wing/Rotor and Rotor/Rotor Interactions Present in Tilt-Rotor Aircraft, Presented at the International Conference of Rotorcraft Basic Research, Army Research Office, Februar 1985, Vertica Vol.11 No.4 pp 731-749, 1987
- [8] R. Behr, S. Wagner, A Vortex-Lattice Method for the Calculation of Vortex Sheet Roll up and Wing Vortex

Interactions, Notes on Numerical Fluid Mechanics Volume 25, p. 1-14, Friedrich Vieweg&Sohn, Braunschweig/Wiesbaden 1989

[9] K.Bartie,H.Alexander,M.Mc Veigh,S.i.a.Mon,H.Bishop, Hover Performance Tests of Baseline Metal and Advanced Technology Blade (ATB) Rotor Systems for the XV-15 Tilt Rotor Aircraft, NASA Contractor Report 177436, Oktober 1986

[10] Ch. Urban, Ein Wirbelgitterverfahren zur Berechnung von Interferenzeffekten zwischen Tragflächen und freien Wirbelschichten bei Unterschallströmung, Uni Bw, Fakultät LRT, Dissertation, April 1988

[11] Dave P. Witkowski, Alex K.H. Lee and John P.Sullivan, Aerodynamic Interaction Between Propellers and Wings, AIAA 26th Aerospace Sciences Meeting, January 11-14, 1988 / Reno Nevada

[12] Luis L.Miranda,James E.Brennan, Aerodynamic Effects of Wingtip Mounted Propellers and Turbines, AIAA 86-1802, 1986

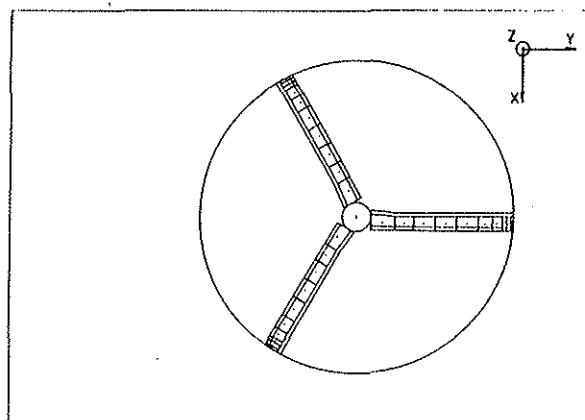


Figure 2. Discretisation of the isolated rotor (XV-15)

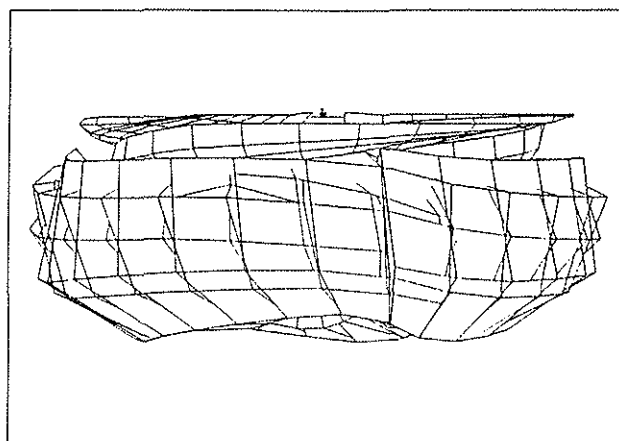


Figure 3. Created wake "bulb"

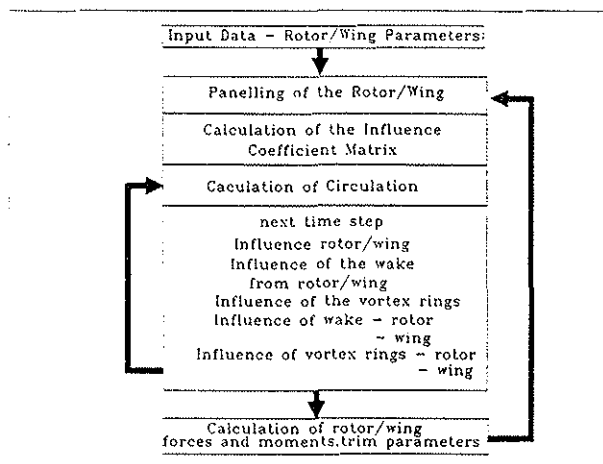


Figure 1. Rotor/wing interference calculation schematic

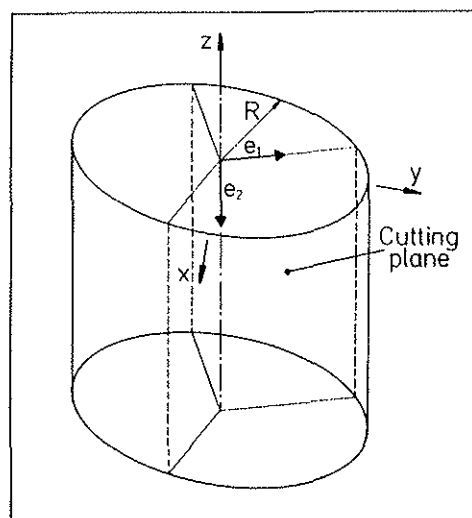


Figure 4. Wake Model represented by cutting planes

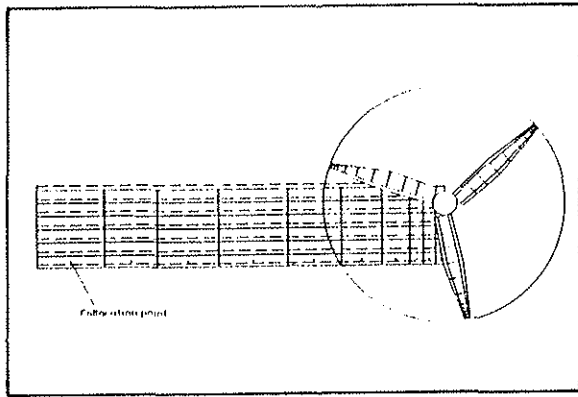


Figure 5. VLM discretisation for rotor/wing in hover

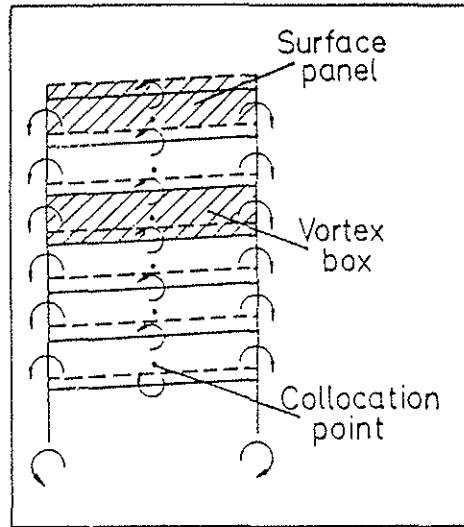


Figure 8. Discretisation for the wing

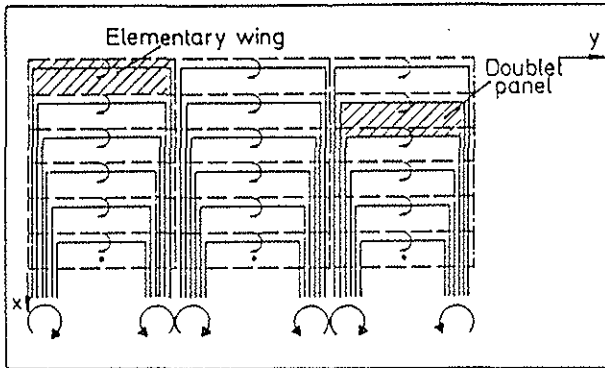


Figure 6. Horseshoe vortex representation for the wing in hover

Table 1: Conditions and configurations analyzed			
Flight condition	Isolated rotor XV-15	rotor+wing (Clark) XV-15	rotor+wing XV-15
Hover	$\Theta_3 = 12$	$\Theta_3 = 45$	
	$\Theta_1 \text{ nonlinear}$	$\Theta_1 = -40$	
Forward Flight			$\Theta_3 = 58$
			$\Theta_1 \text{ nonlinear}$

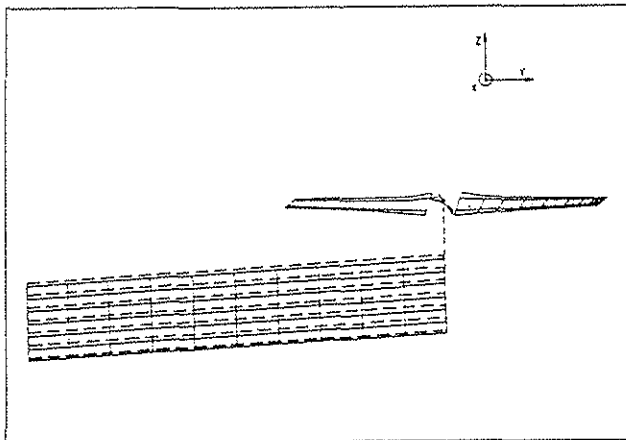


Figure 7. VLM discretisation for rotor/wing in forward flight

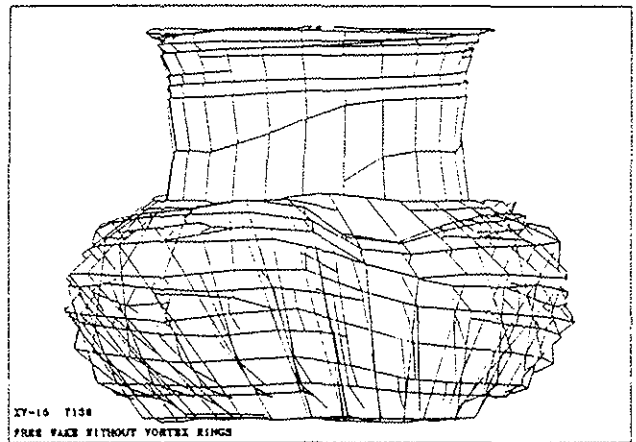


Figure 9a. Wake for the isolated rotor in hover

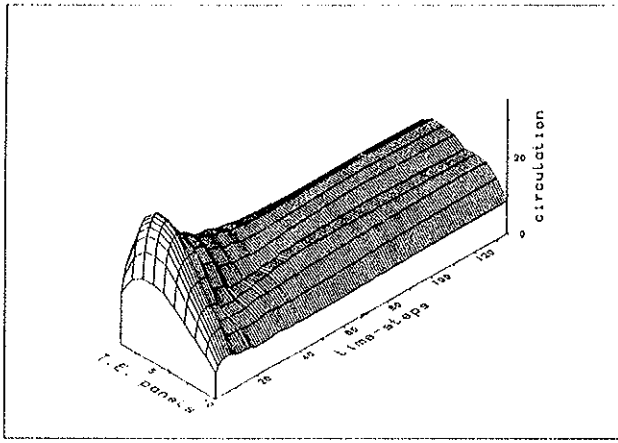


Figure 9b. Circulation distribution of the single rotor blade

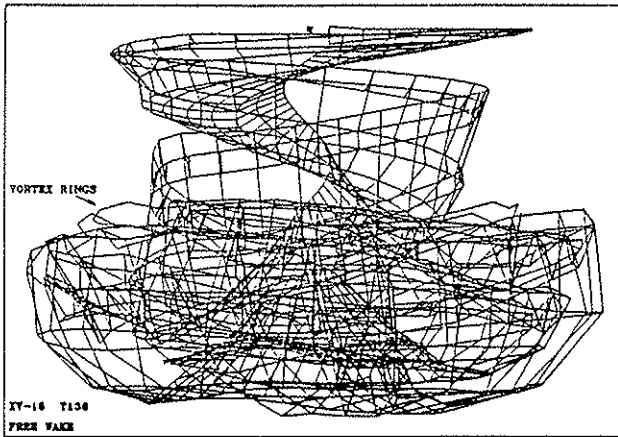


Figure 10. Single rotor wake with vortex rings

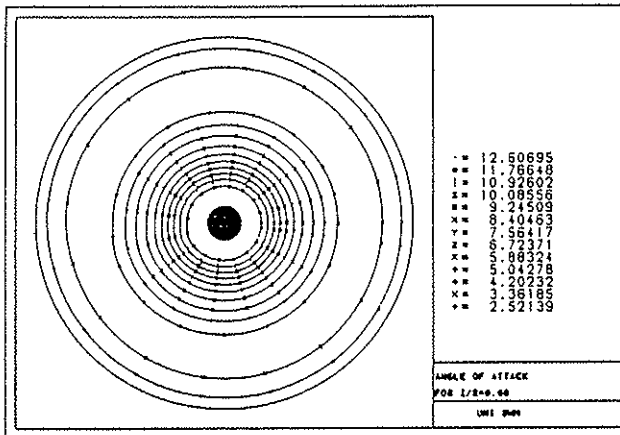


Figure 11. Angle of attack for the XV-15 in hover

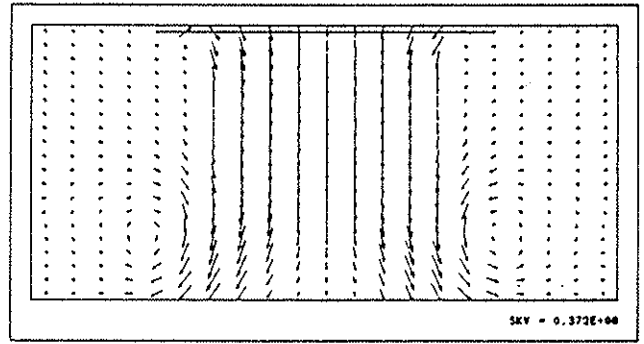


Figure 12. Flow field under the rotor

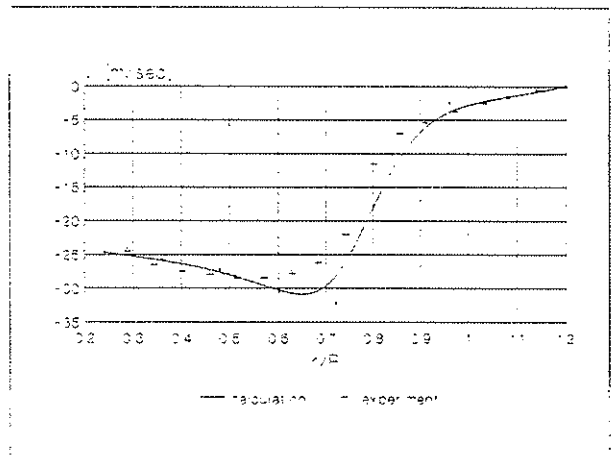


Figure 13. Calculated and measured induced velocity distribution

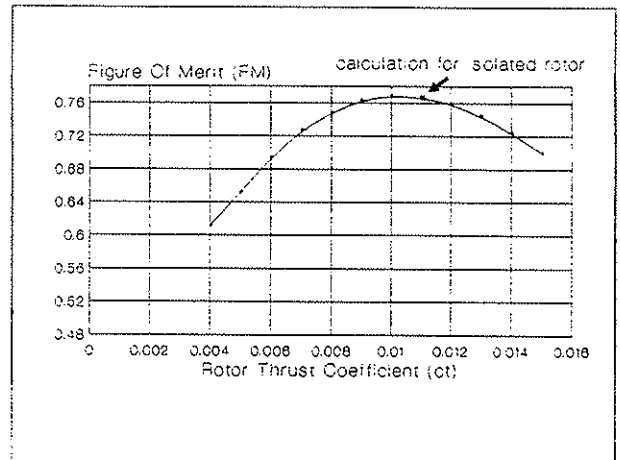


Figure 14. Figure of merit for the XV-15 in hover

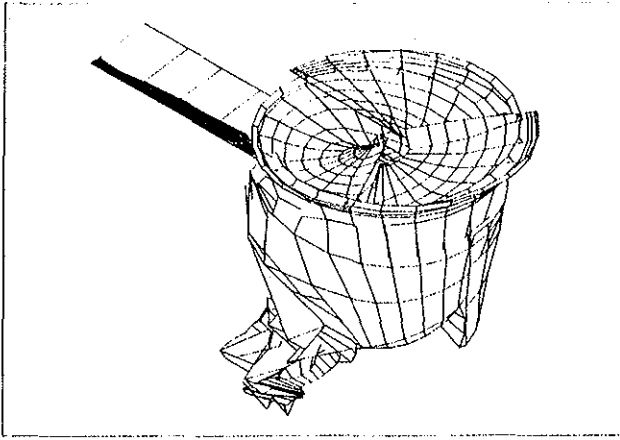


Figure 15a. Wake of rotor/wing in hover case

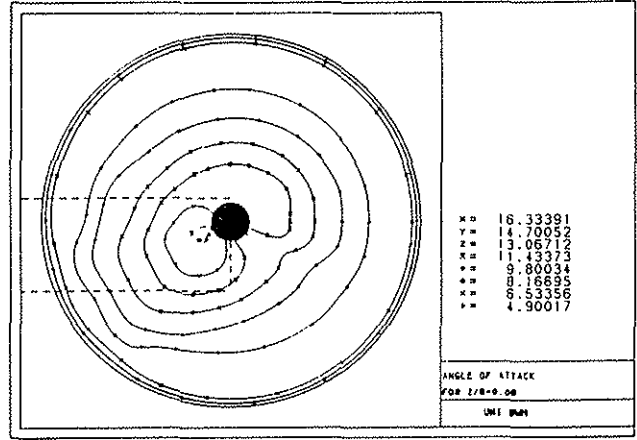


Figure 17a. Angle of attack for wing / rotor in hover

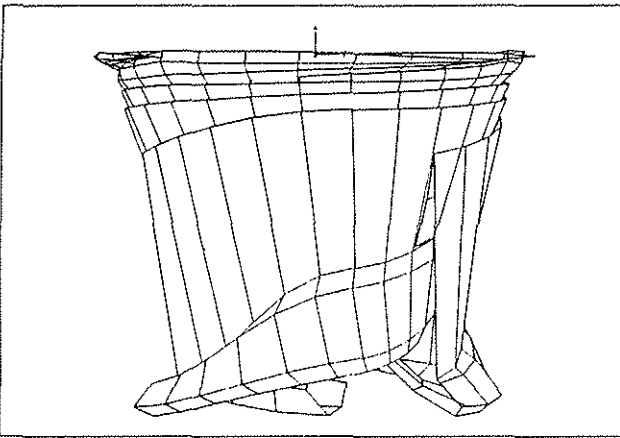


Figure 15b. Single rotor wake

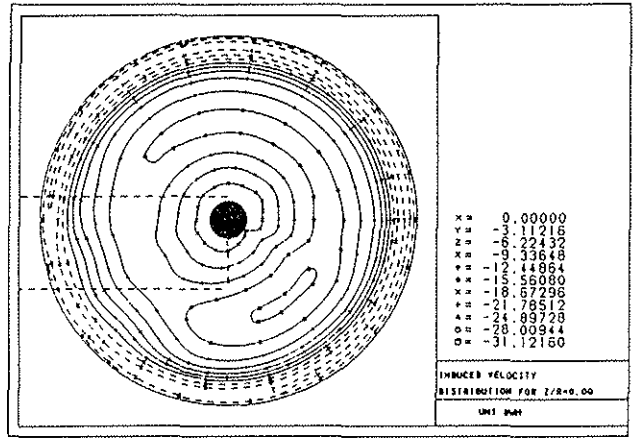


Figure 17b. Induced velocity distribution for rotor/wing

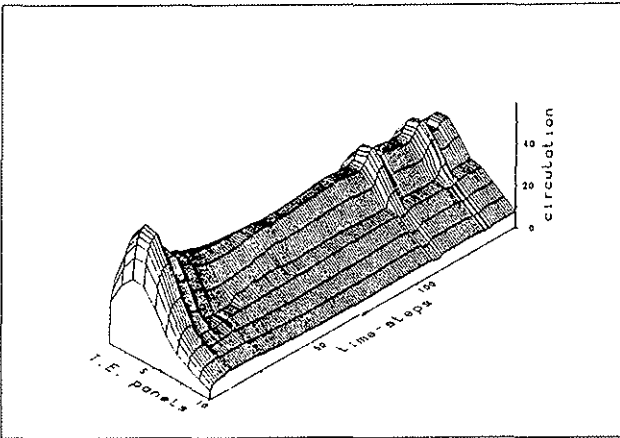


Figure 16. Rotor circulation distribution for rotor / wing in hover case

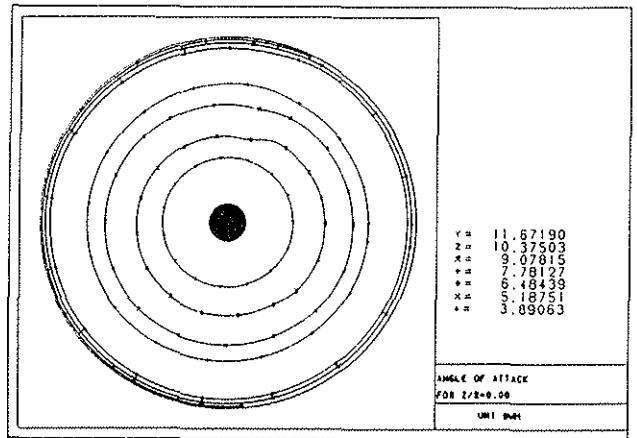


Figure 18a. Angle of attack for the isolated rotor in hover

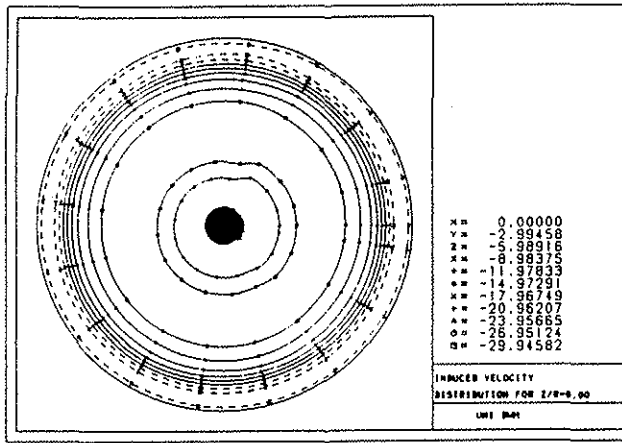


Figure 18b. Induced velocity distribution of the isolated rotor

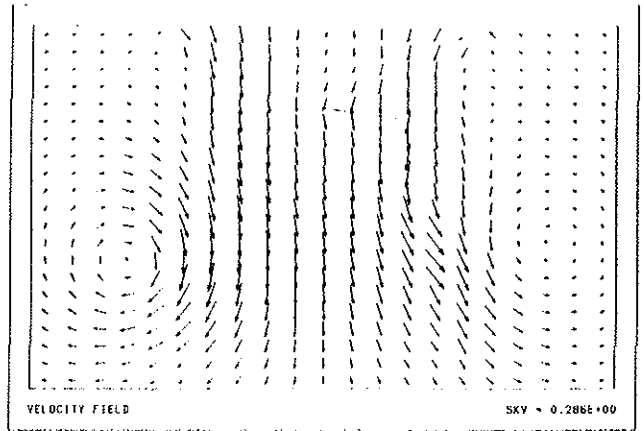


Figure 20. Velocity field for the hover case of rotor / wing

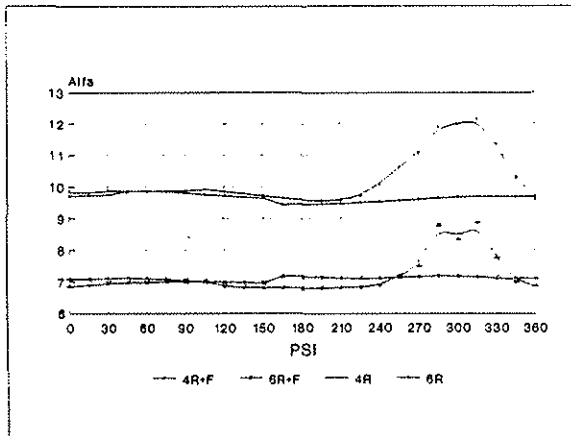


Figure 19a. Azimuthal angle of attack of the rotor over the wing

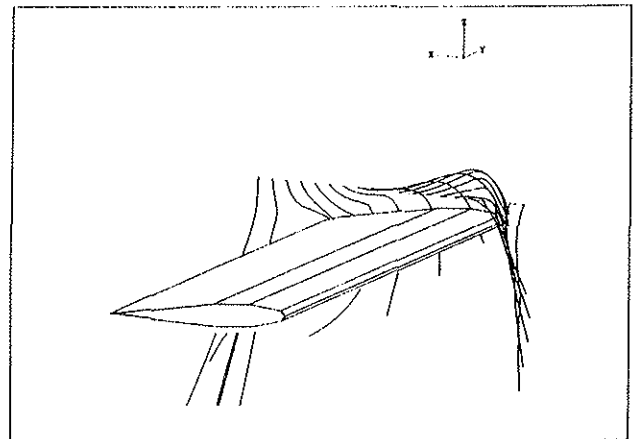


Figure 21. Streamlines at the wing tip

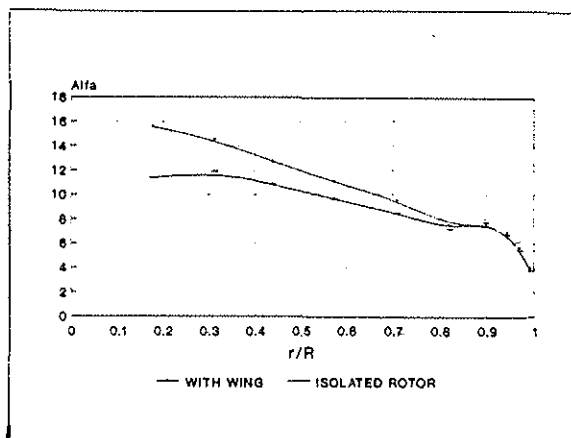


Figure 19b. Radial angle of attack at the wing position

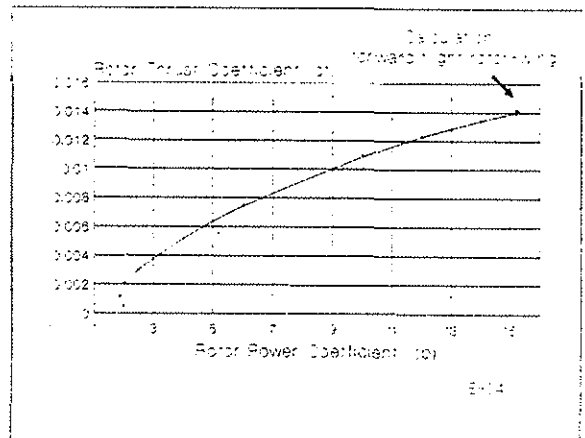


Figure 22. Measured and calculated power coefficient in forward flight

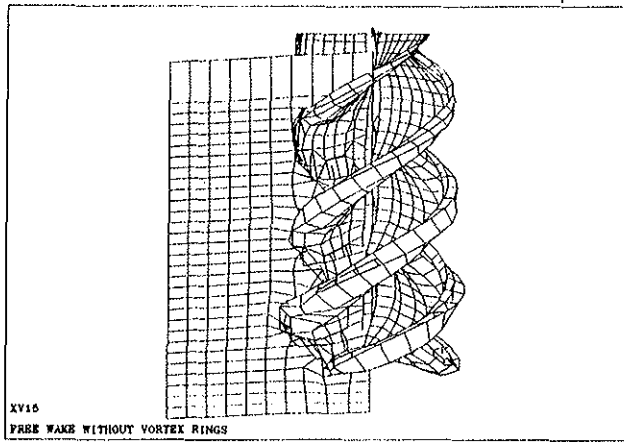


Figure 23a. Wake for rotor/wing in forward flight

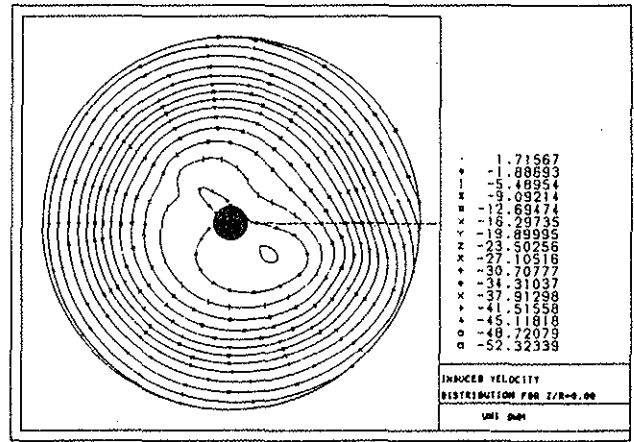


Figure 24b. Induced velocity distribution of the rotor

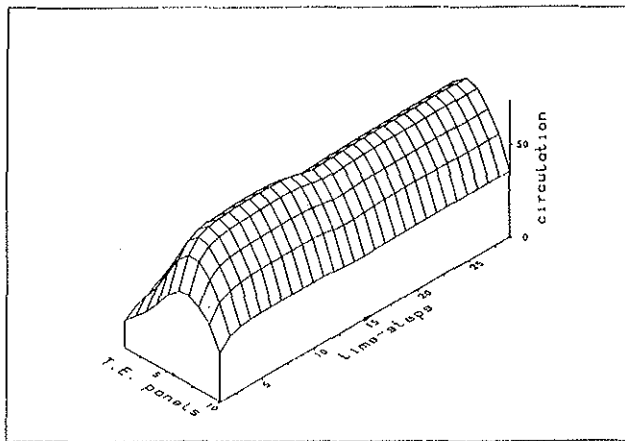


Figure 23b. Rotor circulation distribution for rotor/wing

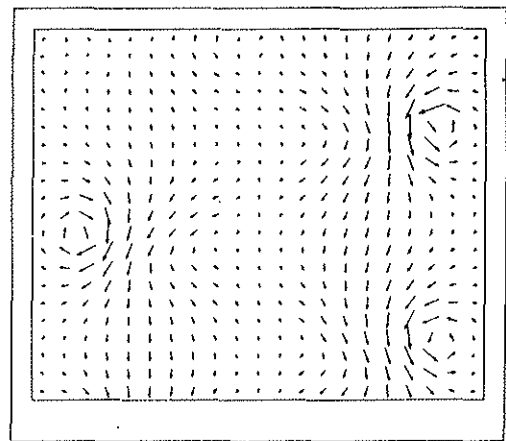


Figure 25. Flow vectors in y-z plane

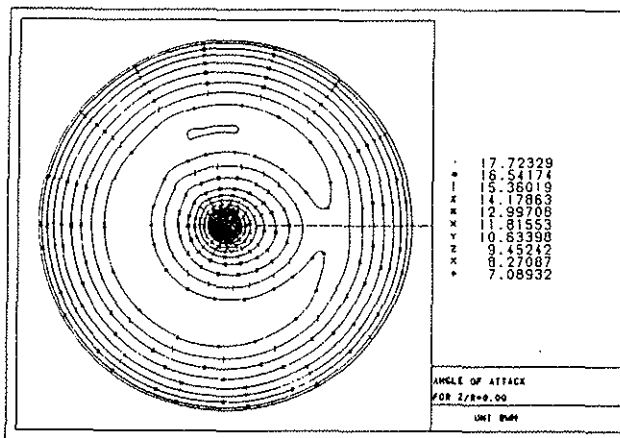


Figure 24a. Angle of attack for the rotor in forward flight

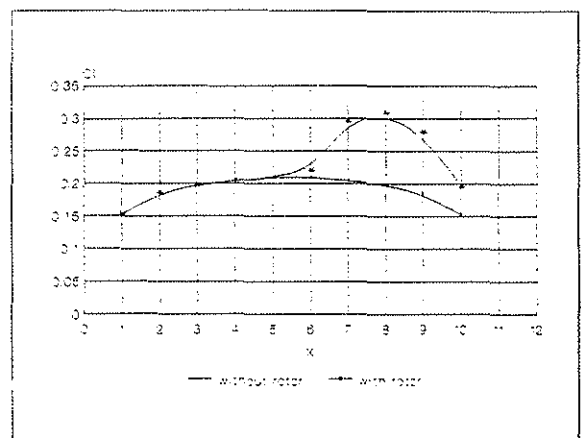


Figure 26. Wing loading with/without rotor in forward flight